Solar-Terrestrial Physics. 2025, vol. 11, iss. 4, pp. 14–28. DOI: 10.12737/stp-114202504.© 2025
S.N. Ponomarchuk, N.A. Zolotukhina, V.I. Kurkin, A.Yu. Belinskaya, V.P. Grozov, A.V. Oinats, A.I. Poddelsky, A.V. Podlesnyi, M.V. Cedrik.
Published by INFRA-M Academic Publishing House

DOI: 10.12737/stp-114202504

Received April 15, 2025
Accepted June 02, 2025

EFFECTS OF THE MAY 10–13, 2024 MAGNETIC STORM IN THE ASIAN REGION OF RUSSIA FROM IONOSPHERIC SOUNDING WITH A CONTINUOUS CHIRP SIGNAL

S.N. Ponomarchuk
Institute of Solar-Terrestrial Physics SB RAS, Irkutsk, Russia, spon@iszf.irk.ru

N.A. Zolotukhina
Institute of Solar-Terrestrial Physics SB RAS, Irkutsk, Russia, zolot@iszf.irk.ru

V.I. Kurkin
Institute of Solar-Terrestrial Physics SB RAS, Irkutsk, Russia, kurkin@iszf.irk.ru

A.Yu. Belinskaya
Trofimuk Institute of Petroleum Geology and Geophysics SB RAS, Novosibirsk, Russia, belinskayaay@ipgg.sbras.ru

V.P. Grozov
Institute of Solar-Terrestrial Physics SB RAS, Irkutsk, Russia, grozov@iszf.irk.ru

A.V. Oinats
Institute of Solar-Terrestrial Physics SB RAS, Irkutsk, Russia, oinats@iszf.irk.ru

A.I. Poddelsky
Institute of Cosmophysical Research and Radio Wave Propagation FEB RAS, Paratunka, Russia, podd-igor@yandex.ru

A.V. Podlesnyi
Institute of Solar-Terrestrial Physics SB RAS, Irkutsk, Russia, pav@iszf.irk.ru

M.V. Cedrik
Institute of Solar-Terrestrial Physics SB RAS, Irkutsk, Russia, mark7cedrick@gmail.com

Abstract. Effects of the May 10–13, 2024 extreme magnetic storm in the Asian region of Russia have been studied using experimental data from vertical and oblique sounding of the ionosphere with a continuous chirp signal. Features of ionospheric disturbances induced by the magnetic storm have been revealed: the long-lasting negative ionospheric disturbance that was manifested as a significant decrease in F2-layer critical frequencies and maximum observed frequencies of radio paths; the absence of HF signal reflections from F-region due to sporadic E_s layer and increased absorption of HF signals; recording of auroral and oblique E_s layers; the long-lasting G-effect during local daytime during which the F1-layer critical frequency exceeded the F2-layer critical frequency; the dusk enhancement of electron density and F2-layer peak height. We have found a correlation of variations in ionospheric parameters and the maximum observed frequencies of HF radio wave propagation modes with spatial location of the main ionospheric trough and the equatorial boundary of the diffuse electron precipitation zone.

Keywords: ionospheric disturbances, radio wave propagation, magnetosphere, ionosphere, main ionospheric trough, diffuse electron precipitation.

INTRODUCTION

Geomagnetic storms that change the structure of the magnetosphere and ionosphere disrupt the operation of technological systems. The probability of disruptions increases with increasing storm intensity, which is most often measured by the K_p [https://www.swpc.noaa.gov/noaa-scales-explanation] and *Dst* indices [Gonzalez et al., 1994; Loewe, Prolss, 1997; Echer et al., 2008].

The magnetic storm that began on May 10, 2024 with minimum *Dst*=–406 nT and maximum K_p=9, called the Mother's Day superstorm [Spogli et al., 2024], is great according to *Dst*≤–350 nT [Loewe, Prolss, 1997] and extreme according to K_p=9. Such storms are very rare. They account for less than 1 % of recorded magnetic storms [Loewe, Prolss, 1997; Collado-Villaverde et al., 2024]. It is essential to examine disturbances of the magnetospheric-ionospheric system during each of such storms in order to create a generalized picture of physical processes in geospace during great storms.

The results of comprehensive analysis of experimental data obtained on October 29 – November 1, 2003 during the great storm known as the Halloween storm are presented in [Panasyuk et al., 2004; Zherebtsov et al., 2005]. The authors have shown that during the storm such structures as the equatorial edge of the auroral oval, the inner edge of the plasma sheet, diffuse and discrete electron precipitation zones, the main ionospheric trough (MIT), and the westward electrojet, usually located in the auroral and subauroral zones, shifted to midlatitudes. In vertical sounding (VS) ionograms, these shifts appeared on October 29–31 as blackout intervals and sporadic E layers of a, s, and f types, partially or completely shielding the F-region of the ionosphere above Moscow (L~2.6) and Irkutsk (L~2.2) [Panasyuk et al., 2004; Zherebtsov et al., 2005]. Along oblique sounding (OS) paths, changes in the po-

sition of MIT and the diffuse electron precipitation zone during the storm caused considerable variations in maximum observed frequencies (MOFs) of radio wave propagation modes, deviation of signal propagation paths from the great circle arc, and appearance of anomalous diffuse signals with delays exceeding the delays of the main propagation modes [Kurkin et al., 2004; Uryadov et al., 2004; Uryadov et al., 2005].

The next great storm that began on November 20, 2003 was also accompanied by strong ionospheric disturbances giving rise to shielding E_s layers and long blackout intervals in VS ionograms recorded in Eastern Siberia at midlatitudes [Zherebtsov et al., 2005]. Reflections from the E_s layer were clearly seen in ionograms in Norilsk (L~5.5), Zhigansk (L~4.4), and Yakutsk (L~3.3) and were less pronounced in ionograms in Irkutsk (L~2.2). Mishin et al. [2018], using the magnetogram inversion technique, have shown that on November 20 at 16:30–22:30 UT (the last six hours of the storm main phase) the equatorial boundary of the auroral oval repeatedly shifted to latitudes below the latitude of Irkutsk. During the given period, the Irkutsk station was in the midnight-dawn sector (23:30–05:30 LT). At the same time, the VS ionograms obtained in the dusk sector (16:30–22:30 LT) at latitudes from 37.1° N (L~1.3) to 51.5° N (L~2.2) revealed a rise and expansion of the F-region of the ionosphere and its shielding by type a, k, r E_s layers [Blanch et al., 2005]. Long blackout intervals were recorded along oblique sounding paths during the storm main phase.

According to minimum *Dst* (–406 nT), the May 2024 storm is the sixth of the ten great storms observed from the beginning of 1957 to November 2024, but the first with maximum A_p=271. The A_p index is equal to the average of the eight three-hour values of the *ap* index obtained during the day, which is the input parameter in the model for calculating the invariant latitude (Φ) of the MIT bottom, presented in [Deminov, Shubin, 2018]. Potential uses of this model for estimating the location of MIT for weak, moderate, and strong magnetic storms are discussed, for example, in [Ponomarchuk, Zolotukhina, 2024]. The high value of A_p=271 suggests that during the May 2024 storm a decrease in the invariant latitude of the MIT bottom might have been more significant than during other great storms. Spogli et al. [2024] have demonstrated that on May 10, during the Mother's Day superstorm main phase, decreases in the F2-layer critical frequency (f_oF2), total electron content (TEC), and blackout intervals, characteristic of MIT, were observed in Italy at latitudes 37.9°–41.8° N.

In this paper, we examine magnetic storm effects by analyzing data from vertical and oblique ionospheric sounding with a continuous chirp signal [Podlesny et al., 2013; Kurkin et al., 2024a], using empirical models of invariant latitudes of MIT bottom [Deminov, Shubin, 2018] and equatorial boundary of the diffuse precipitation zone of ≥100 eV electrons [Kamide, Winningham, 1977], as well as models of magnetospheric convection field strength E_c [Burke et al., 2007]. We also employ data on spatial distribution of total electron content. The main purpose of this work is to study the magnetosphere-ionosphere coupling effect on radio wave propagation conditions in the Asian region of Russia during the great magnetic storm on May 10–13, 2024.

1. GEOMAGNETIC DISTURBANCES AND THEIR INTERPLANETARY SOURCES

1.1. Manifestations of the storm in geomagnetic indices

According to increases in K_p to 8 and *Dst* to 66 nT (Figure 1, *a*), the great magnetic storm of interest began on May 10 at 15:00–18:00 UT. The K_p and *Dst* values were taken from the websites [https://kp.gfz-potsdam.de/en/data] and [https://wdc.kugi.kyoto-u.ac.jp/dst_provisional/index.html] respectively. The monotonous increase in *Dst* from 1 nT at 13–14 UT to 66 nT at 17–18 UT on May 10 allows us to assume that the 3-hr interval 15:00–18:00 UT, when *Dst* was positive, is the storm initial phase. Variations in 1-min *SYM-H* values compared in Figure 1 *a* with *Dst* variations suggest that a sharp increase in *SYM-H* from 10 to 88 nT occurred on May 10 for 9 min (at 17:06–17:15 UT). In time, this change corresponds to an increase in the solar wind dynamic pressure P_{sw} by 31 nPa, which is typical for storms with sudden commencement. The *SYM-H* values were positive for 47 min, until 17:53 UT. After that, for ~9 hrs of the storm main phase, *Dst* and *SYM-H* decreased, reaching minimum *Dst*=–406 nT and *SYM-H*=–518 nT by 02:30 UT on May 11. Then, within 24 hours, until ~02:30 UT on May 12, the *Dst* index increased relatively rapidly, which is peculiar to the storm early recovery phase [Daglis, 2001]. The late recovery phase of the storm ended on May 13 at 18:30 UT.

Maximum K_p=9 was recorded on May 11 at 00–03 UT (last 3 hrs of the storm main phase) and at 09–12 UT (early recovery phase). In the second of these periods, the *Dst* index increased by 100 nT, which, as shown in [Iyemori, Rao, 1996], can occur during substorms due to current attenuation in the magnetotail neutral sheet.

The time intervals of the storm phases, determined by variations in *SYM-H* (initial and main phases) and *Dst* (recovery phases) are listed Table.

1.2. Main characteristics of the interplanetary storm source

The storm in question was generated by a complex interplanetary inhomogeneity produced by a series of coronal mass ejections. On [https://cdaw.gsfc.nasa.gov/CME_list/], seven of them are classified as halo-type coronal mass ejections. Figure 1, *b* illustrates variations in some parameters of this inhomogeneity. The storm initial and main phases are marked with gray rectangles in this and following Figures; the end moments of the storm early and late recovery phases are indicated by vertical gray lines.

The 47-min initial phase of the storm developed under the effect of its leading region in which the solar wind (SW) velocity (V_{sw}~600 km/s), ion concentration

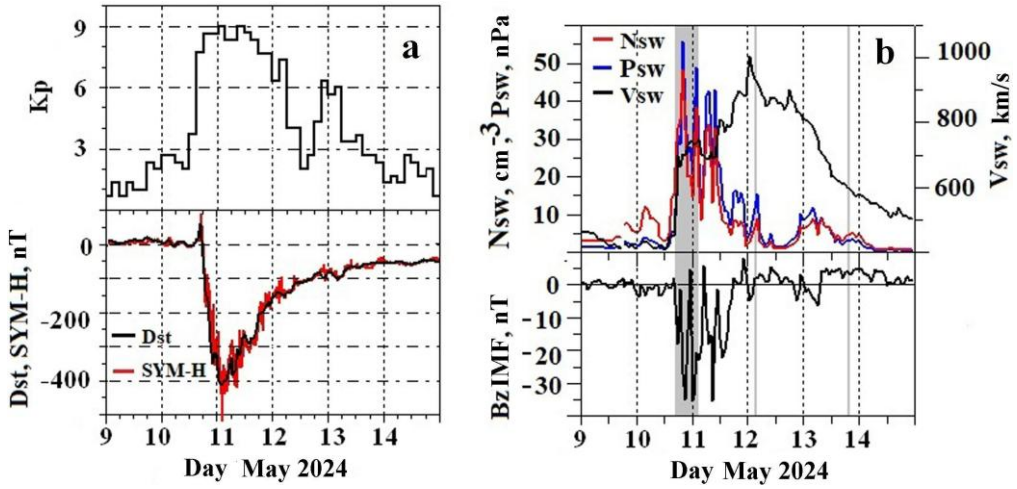

Figure 1. Variations in the K_p, *Dst*, and *SYM-H* indices on May 09–14, 2024 (*a*) and corresponding variations in hourly average interplanetary medium parameters (*b*): SW ion concentration (N_{sw}), dynamic pressure (P_{sw}), and velocity (V_{sw}), as well as IMF B_z. In panel *b* and in Figures 3, 5, 7–9, the storm initial and main phases are marked with a gray rectangle; the end moments of its early and late recovery phases are indicated by vertical gray lines

Storm phase intervals on May 10–13, 2024

Phase	Beginning		End		Extremums	
	day/month	UT	day	UT	*Dst*, nT	K_p
Initial	10.05	17:06	10.05	17:53	66	8–
Main	10.05	17:54	11.05	02:14	–406	9
Early recovery	11.05	02:30	12.05	02:30		
Late recovery	12.05	02:30	13.05	18:30		

(N_{sw}~30 cm^{-3}), and dynamic pressure (P_{sw}~18 nPa), as well as the interplanetary magnetic field (IMF) modulus B_t~7 nT were much higher than in slow SW in front of the region (Figure 1, *b*). The IMF azimuthal (B_y) and vertical (B_z) components in it were –2 and –6 nT.

The storm main phase is associated with the SW region having V_{sw}~700 km/s, the largest values of N_{sw}, P_{sw}, and a predominantly negative vertical IMF component, which twice decreased to extreme values B_z=–35 and –35.3 nT for this event.

In the interplanetary source responsible for the storm early recovery phase, the velocity increased to maximum for this event, V_{sw}~1000 km/s. N_{sw} and P_{sw} noticeably decreased, and the negative B_z component gradually became positive by the end of the early recovery phase. Further weakening of negative B_z and decreases in N_{sw}, P_{sw}, and V_{sw} led to the transition from the storm early recovery phase to the late one.

2. EXPERIMENT AND DATA PROCESSING

ISTP SB RAS in cooperation with IPGG SB RAS and IKIR FEB RAS has organized continuous monitoring of the ionosphere in the Asian region of Russia based on vertical, near-vertical (NVS), and oblique sounding data. The ionospheric sounding is performed by a multifunctional digital ionosonde with a continuous chirp signal, developed at ISTP SB RAS [Podlesny et al., 2013; Kurkin et al., 2024b]. Geometry of OS paths is depicted in Figure 2. Transmitting stations are located near Irkutsk (52.88° N, 103.26° E), Magadan (60° N, 150.7° E), Khabarovsk (47.6° N, 134.7° E), Novosibirsk (55° N, 83° E), and Norilsk (69.4° N, 88.4° E). Receiving stations are the Irkutsk station (Tory village (51.8° N, 103° E), Buryatia) and the Novosibirsk station (55° N, 83° E). Analysis of OS data allows us to examine the effect of the dynamics of large-scale structures (the main ionospheric trough, the diffuse electron precipitation zone) on variations in ionospheric characteristics and HF signal propagation during geomagnetic storms [Ponomarchuk, Zolotukhina, 2024; Kurkin et al., 2024a]. Vertical sounding of the ionosphere is performed at the Irkutsk and Novosibirsk stations. Quick mode (with a step of 1 min or less) of ionospheric VS and NVS can implement algorithms for calculating the velocity of ionospheric disturbances with scales of tens of kilometers [Laryunin et al., 2024] and to investigate the morphological features of such disturbances. Sounding with a step of 5 min along single-hop OS paths makes it possible to study characteristics of traveling ionospheric disturbances with spatial scales of hundreds of kilometers under various heliogeophysical conditions in the subpolar and mid-latitude ionosphere [Kurkin et al., 2024b].

During the May 2024 storm, the transmitting stations in Norilsk and Khabarovsk did not work for technical reasons, so experimental studies of radio wave propagation were carried out along the OS radio paths Magadan—Irkutsk (length D=3034 km, midpoint longitude λ=124.21° E, invariant latitude Φ=53.39°), Magadan—Novosibirsk (D=3901 km, λ=114.2° E, Φ=57.77°), and Novosibirsk—Irkutsk (D=1372 km, λ=93.4° E, Φ=50.17°).

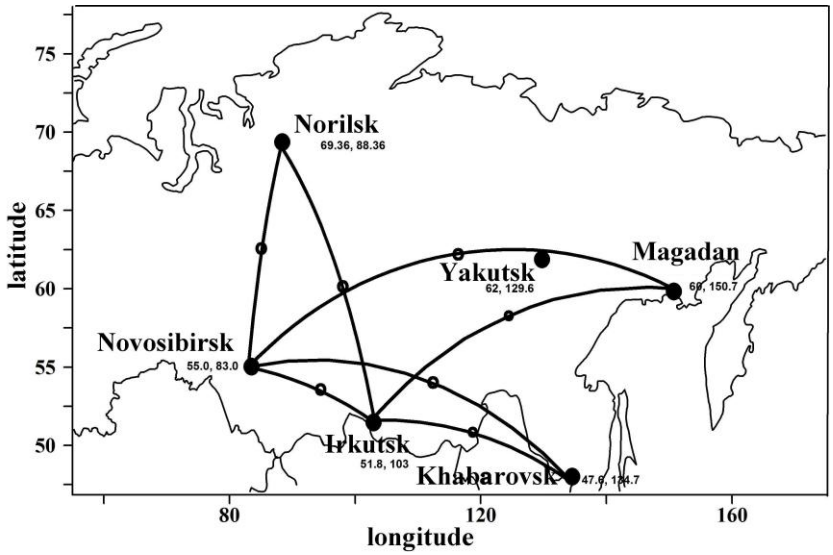

Figure 2. Oblique sounding paths in the Asian region of Russia

Automatic processing and interpretation of ionograms were used for preliminary analysis of a large number of high-frequency and low-frequency ionograms (about 25000) [Grozov et al., 2012; Ponomarchuk et al., 2023; Ponomarchuk, Grozov, 2024]. From the results of processing and interpretation of high-frequency ionograms, we identified the height-frequency characteristic (HFC). The HFC track was employed to calculate critical frequencies and minimum reflection heights for each ionospheric layer, as well as the vertical plasma frequency profile $f_e(h)$ [Mikhailov, 2000]. From the $f_e(h)$ profile, we determined the F2-layer parameters: the critical frequency and the peak height h_mF2. We also distinguished the track of the sporadic E_s layer in the VS ionogram and its parameters (height, critical frequency, and shielding frequency of F reflections). The E_s-layer type was not identified.

During the long-lasting negative ionospheric disturbance accompanying the magnetic storm, there was a G effect in VS ionograms — shielding of the F2 layer by the F1 layer during local daytime hours, which led to incorrect identification of the signals reflected from these layers. Therefore, the data from automatic processing of ionograms was adjusted interactively.

Using the results of processing of VS and OS ionograms, we plotted time dependences of critical frequencies of the ionospheric layers F2 (f_oF2), F1 (f_oF1), E (f_oE), E_s (f_oE_s), and maximum observed frequencies of propagation modes for signals reflected from the ionospheric layers F2 (MOF1F2, MOF2F2), F1 (MOF1F1), E (MOF1E), and E_s (MOF1E_s, MOF2E_s). The term "propagation mode" describes radio wave propagation by reflection (single, double, etc.) from ionospheric layers — 1E, 1E_s, 1F1, 1F2, 2F2, etc. Detailed identification of signals reflected from the ionosphere and analysis of radio wave propagation and scattering were made using experimental ionograms. We also applied empirical models of invariant latitudes of the MIT bottom and the diffuse precipitation boundary (DPB), and a model of magnetospheric convection field strength.

3. IONOSPHERIC STORM MANIFESTATIONS IN VS AND OS DATA

Geomagnetic storms are accompanied by ionospheric storms of different types, which alter HF radio wave propagation conditions. The spatial location of large-scale structures, primarily MIT and the diffuse electron precipitation zone, has the most significant effect on radio wave propagation. It is known that the main role in forming large-scale structures of the magnetosphere-ionosphere system, such as the plasmapause, the inner edge of plasma sheet, equatorial and polar boundaries of the auroral oval, is played by the electric field of magnetospheric convection [Sergeev, Tsyganenko, 1980; Nishida, 1980]. Strengthening of the magnetospheric convection field causes the inner plasma sheet boundary and the outer plasmasphere boundary to shift deep into the magnetosphere; and their ionospheric projections, to the equator. Accordingly, MIT located between the auroral oval and the plasmapause and the electron density irregularities characteristic of MIT and affecting HF radio wave propagation shift to lower latitudes. The magnetospheric convection field strength is determined by near-Earth interplanetary medium parameters. In this work, its value was calculated from V_{sw}, P_{sw}, IMF B_y and B_z [Burke et al., 2007]. The MIT position was estimated by the empirical model of invariant latitude of the MIT bottom [Deminov, Shubin, 2018]. To estimate the location of the diffuse precipitation zone of ≥100 eV electrons, which cause the electron density to increase in the F-region [Fang et al., 2008], we computed the latitude of the equatorial boundary of the diffuse precipitation zone [Kamide, Winningham, 1977]. Under disturbed conditions, electron precipitation leads to an increase in the F2-layer electron density near the MIT polar wall [Galperin et al., 1977; Khalipov et al., 1977]. During the post-midnight hours under high geomagnetic activity conditions, additional regions of increased electron density can form inside MIT — ridges of electron

density [Besprozvannaya, Benkova, 1988; Zherebtsov et al., 1988], as well as structures of field-aligned small-scale irregularities — "screens" in the terminology used in [Möller, 1974; Pilkington et al., 1975]. We employed TEC maps to estimate the total electron content [https://cdaweb.gsfc.nasa.gov].

3.1. Ionospheric disturbances according to VS data

Ionospheric disturbances during the May 2024 magnetic superstorm were most pronounced in the data from vertical sounding of the ionosphere with a continuous chirp signal. The short time step of high-frequency ionograms (from 1 min to 15 s) and the high spatial and frequency resolution make it possible to thoroughly examine dynamic processes in the ionosphere and to identify features of ionospheric parameter variations.

3.1.1. Novosibirsk station

Figure 3 illustrates variations in critical frequencies of the ionospheric layers F2, F1, and E_s, invariant latitudes of the MIT bottom and DPB at 90° E, and the magnetospheric convection field strength E_c on May 9–14, 2024, as well as VS ionograms from the Novosibirsk station for May 10–11, 2024. Black dots in top panels mark experimental values of critical frequencies under disturbed conditions obtained from processing of VS ionograms; red lines indicate F2- and F1-layer critical frequencies for the quiet day on May 9, 2024; the blue

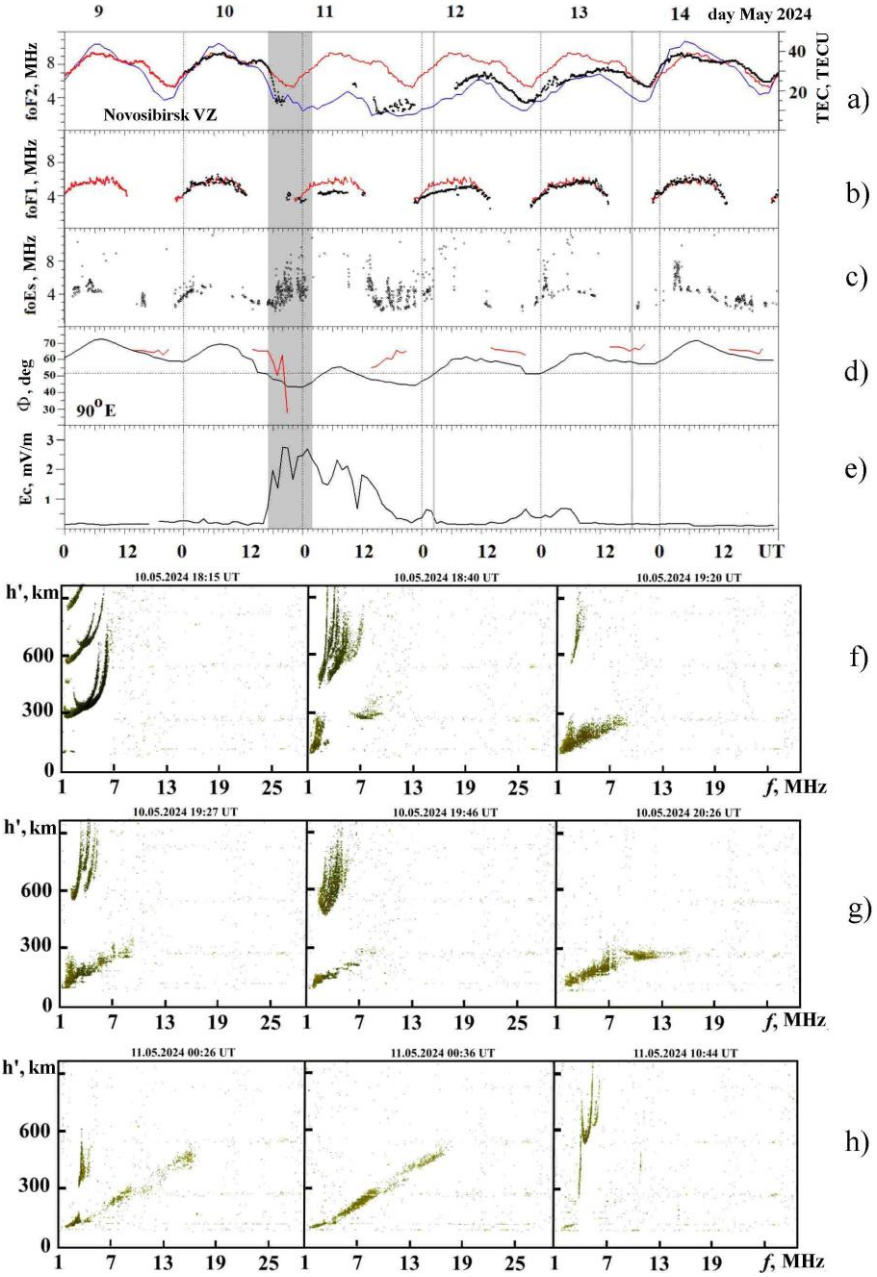

Figure 3. Variations in TEC (blue line), current (black dots) and background (red line) values of f_oF2 (*a*), f_oF1 (*b*), f_oE$_s$ (*c*); variations in invariant latitudes of the MIT bottom (black line) and DPB (red line) at 90° E (*d*), and in the magnetospheric convection field strength E_c (*e*) observed on May 9–14, 2024; VS ionograms received at the Novosibirsk station on May 10–11, 2024 (*f–h*)

line, the results of determination of TEC from maps at a point with coordinates 55° N, 90° E [https://cdaweb.gsfc.nasa.gov].

During the storm main and recovery phases, a long-lasting negative ionospheric disturbance occurred which manifested itself in a significant decrease in the F2-layer critical frequencies (Figure 3, *a*). The ionospheric disturbance was caused by MIT displacement and an increase in the rate of oxygen ion recombination due to a change in the neutral atmosphere composition and a rise in the upper atmosphere temperature during geomagnetic storms [Prölss et al., 1991; Pavlov, 2011]. Extreme values of relative deviations of critical frequencies from background values by ~76 % were observed on May 11. Large decreases in the critical frequency were recorded in those time periods in which the MIT bottom, calculated by the model [Deminov, Shubin, 2018], was located south of the VS station, and f_oF2 decreased to 2–3 MHz, which is typical of MIT [Pirog et al., 2009]. At the same time, the F1-layer critical frequencies also decreased during the storm main and early recovery phases (May 11 and 12). Their extreme deviations from background values were ~25 %. The negative ionospheric disturbance lasted until May 14.

The ionograms recorded at the Novosibirsk station are presented in Figure 3, *f–h*. The magnetic storm began on May 10 at 17:06 UT (see Table). During the main phase, the magnetospheric convection field increased significantly, leading to a shift of MIT and DPB to midlatitudes, including the latitude of the VS station in Novosibirsk (Figure 3, *d*). In Figure 3, the invariant latitude of the Novosibirsk station is denoted by the horizontal dotted line. Manifestations of ionospheric disturbances in VS ionograms from the Novosibirsk station began at 18:15 UT when weak spread-F signals were detected. Later, in the ionograms along with regular signals there are additional diffuse signals reflected both from the MIT polar wall and from the E_s layer. The F2-layer critical frequencies decrease, and its maximum heights increase, which suggests that the VS station is located in the MIT zone [Benkova et al., 1993]. The ionogram at 18:40 UT in Figure 3, *f* illustrates the structure of reflected signals in the case of passage of MIT and the diffuse electron precipitation zone through the zenith transmission sector of the VS station. In addition to the main vertical sounding signals, the ionogram contains diffuse signals corresponding to off-angle reflections from the MIT polar wall. Particle precipitation at the inner plasma sheet boundary also leads to the formation of an auroral E_s layer and to the development of strong plasma turbulence giving rise to small-scale field-aligned irregularities by which bistatic backscattering of radio waves occurs which form oblique reflections from the E layer — oblique E_s [URSI Handbook ..., 1977]. Ionograms with oblique E_s layers are presented in Figure 3, *f–h*. The ionogram on May 10 at 19:46 UT in Figure 3, *g* shows the time when the VS station in Novosibirsk was in the diffuse electron precipitation zone (Figure 3, *d*). A "bunch" of beams is clearly seen for signals reflected from ionospheric irregularities in the F2-region.

Regular signals reflected from the F2 layer were observed on May 10 until 20:20 UT simultaneously with additional diffuse signals reflected from the MIT polar wall and E_s layer. From 20:20 UT on May 10 to 01:00 UT on May 11, there were only traces of reflections from E_s and occasionally from F1 in the ionograms, and only from F1 in the pre-noon sector. Reflection from the F2 layer partially recovered on May 11 between 14:20 and 22:35 UT (the storm early recovery phase) when f_oF2 was extremely low. Reflections from the E_s layer were recorded in the same period.

According to the model results of the invariant latitude of the MIT bottom (Figure 3, *d*), the Novosibirsk VS station was located in the MIT zone in the dusk and night local time sectors on May 10–13. This is supported by the results of reconstruction of the polar oval location from GUVI DMSP SSUSI data [https://ssusi.huapl.edu/gal_edr-aur_cs]; and TEC profiles in selected meridional directions, from maps [https://cdaweb.gsfc.nasa.gov]. Figure 4, *a–d* displays geographical maps with auroral oval boundaries reconstructed from satellite data for 22:10–23:51 UT on May 10, 2024. In fact, on May 10 at 23:51 UT the Novosibirsk VS station is seen to be near the equatorial boundary of the oval, in the MIT region.

Figure 4, *e* plots TEC distribution along the meridians of 85° and 105° E on May 10 at 22:15, 22:30, and 22:45 UT. The plots corresponding to different time points are sequentially shifted along the X-axis by 5 TECU. TEC distributions (Figure 4, *e*) suggest that on May 10 at 22:15–22:45 UT the Novosibirsk station was under the MIT polar wall; and the Irkutsk station, at the MIT bottom latitudes.

A distinctive feature of the ionospheric storm accompanying the magnetic storm considered is the long-term G effect, observed during the daytime hours on May 11 and 12, during which the F1-layer critical frequency exceeded the F2-layer critical frequency: f_oF1>f_oF2 [Polekh et al., 2013, 2015]. The probability of occurrence of the G effect is known to increase with increasing K_p [Deminov et al., 2011]. During the storm recovery phase, the continuous G-effect recording interval at the Novosibirsk station was ~6 hrs (from 02:54 to 09:10 UT) on May 11 and 8 hrs (from 22:45 to 06:45 UT) on May 11–12.

The next feature of the ionospheric storm manifestation in VS data in Novosibirsk and, as will be shown below, in Irkutsk is the short dusk enhancement (dusk effect) of F2-layer electron density and peak height recorded at sunset on May 11 near 10:40 UT (16:40 LT) [Buonsanto, 1995]. This effect is illustrated in Figure 3, *h* by an ionogram obtained on May 11 at 10:44 UT. Note that at this time the convection field strength decreased abruptly to almost an average level under quiet conditions, and then increased sharply (Figure 3, *e*), which might have produced the dusk effect [Tashchilin, Romanova, 2011].

3.1.2. Irkutsk station

Let us examine features of ionospheric disturbances observed at the Irkutsk station. Figure 5 plots variations in the F2-, F1-, E_s-layer critical frequencies and the invariant latitudes of the MIT bottom and DPB at 105° E for May 9–14, 2024, as well as presents VS ionograms obtained at the Irkutsk station on May 10–11, 2024.

As the Novosibirsk station, the Irkutsk station recorded a long-lasting negative ionospheric disturbance during the storm main and recovery phases, which manifested itself as a significant reduction of the F2-layer critical frequencies (Figure 5, *a*). A dramatic decrease in f_oF2 by ~72 % relative to the background values occurred on May 11. At the same time, as at the Novosibirsk station, f_oF1 decreased only during the storm main and early recovery phases (May 11 and 12). An extreme deviation of f_oF1 from the background values was ~25 %. Due to the shift of MIT to the sounding region of the Irkutsk VS station and the higher rate of oxygen ion recombination resulting from a change in the neutral atmosphere composition and a rise in the upper atmosphere temperature [Prölss et al., 1991; Pavlov, 2011], the negative ionospheric disturbance lasted until May 14.

Ionospheric disturbances in VS ionograms from the Irkutsk station appeared as spread-F of signals and a decrease in the F2-layer critical frequency relative to background values at 17:37 UT, i.e. 38 min earlier than at the Novosibirsk station. An ionogram illustrating these phenomena at 17:50 UT is given in Figure 5, *e*. The magnetospheric convection field (see Figure 3, *e*) makes MIT and DPB shift to latitudes close to the invariant latitude of the Irkutsk station (horizontal dotted line in Figure 5, *d*). In addition to regular signals, there are diffuse signals, reflected from the MIT polar wall, in the VS ionograms. The virtual height of signal reflection from the F2 layer increases (Figure 5, *e*–*f*).

The 21:15 UT VS ionogram (Figure 5, *f*) illustrates the structure of reflected signals in the case when the VS station is located in the diffuse electron precipitation zone.

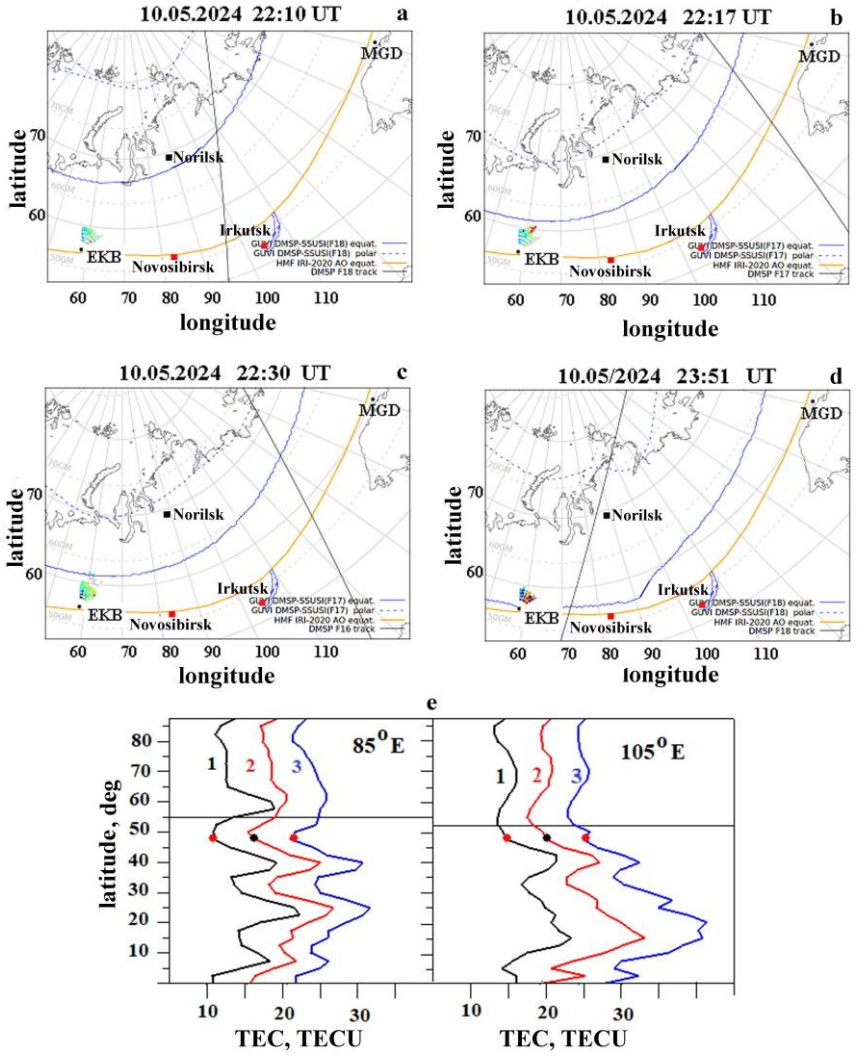

Figure 4. Auroral oval dynamics on May 10, 2024 at 22:10–23:51 UT (*a*–*d*): blue dashed and solid lines represent respectively its polar and equatorial boundaries, constructed from DMSP data; the orange line is its equatorial boundary determined by the IRI-2020 model [Bilitza et al., 2022; Zhang, Paxton, 2008]; the black rectangle marks the location of the Norilsk station; the red rectangles, the Novosibirsk and Irkutsk stations; the inclined line indicates the DMSP satellite path. TEC distribution (*e*) along the meridians of 85° E (left) and 105° E (right) on May 10 at 22:15, 22:30, and 22:45 UT (lines 1, 2, 3 respectively): the horizontal line shows the latitudes of the Novosibirsk station (left) and the Irkutsk station (right); red and black circles denote the MIT bottom latitude according to the model [Deminov, Shubin, 2018]

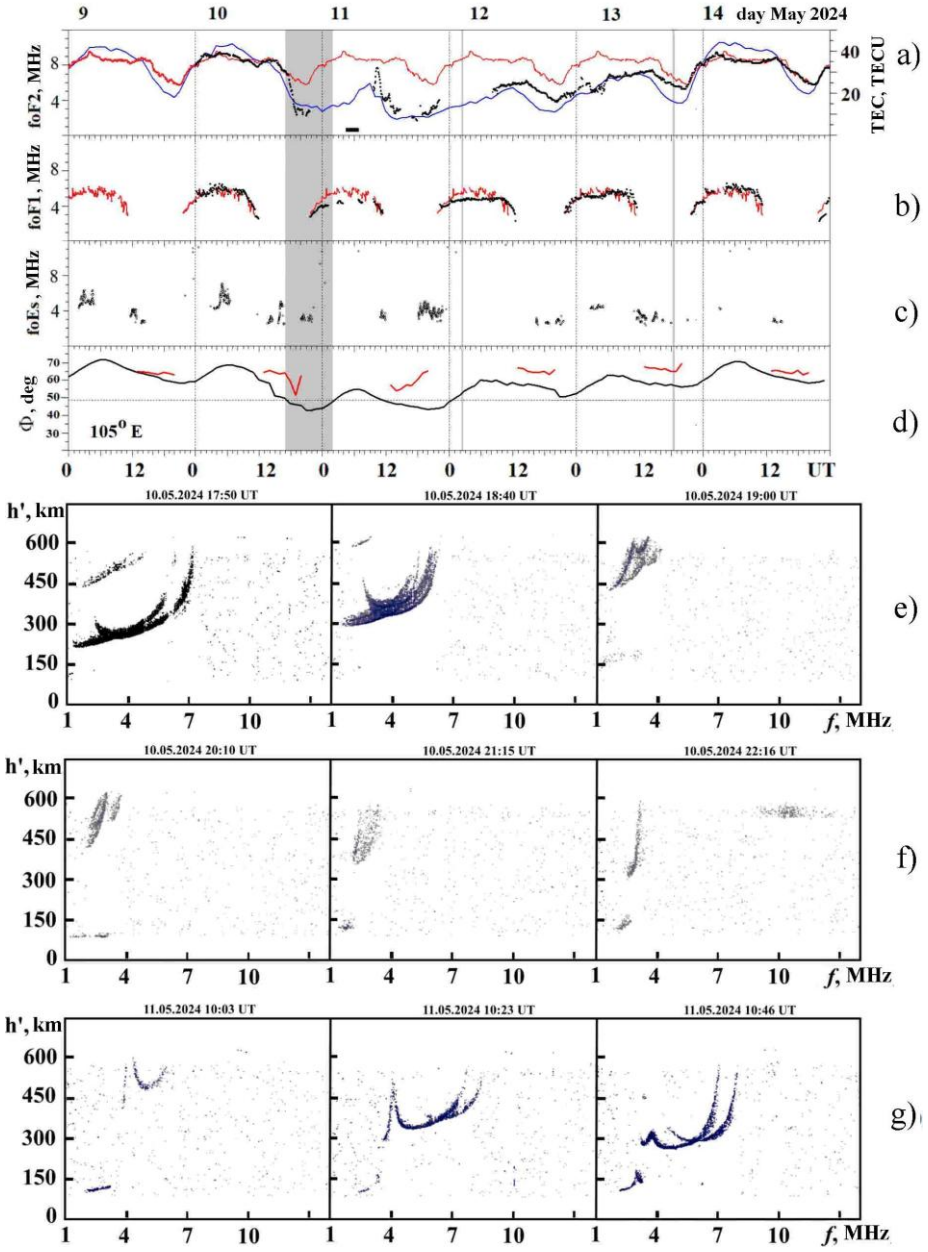

Figure 5. Variations in f_oF2 and TEC (*a*), f_oF1 (*b*), f_oE_s (*c*), invariant latitudes of the MIT bottom and DPB at 105° E (*d*) for May 9–14, 2024; VS ionograms from the Irkutsk station for May 10–11, 2024 (*e*–*g*). Designations are the same as in Figure 3. The black rectangle marks the interval without measurements on May 11, 2024 from 04:30 to 06:49 UT

A "bunch" of beams is seen for signals reflected from ionospheric irregularities in the F2 layer. It is similar in shape to the beam recorded at the Novosibirsk station on May 10 at 19:46 UT (see Figure 3, *g*), but it is observed at lower altitudes and frequencies. Particle precipitation at the inner plasma sheet boundary led to the formation of E_s layers of auroral and delayed types, shown in the ionograms in Figure 5, *f* [URSI Handbook ..., 1977]. No oblique E_s layers were recorded in the ionograms from the Irkutsk station during the magnetic storm. Electron precipitation can result in the formation of ionospheric structures that reflect signals with an almost constant delay. In the 22:16 UT ionogram (Figure 5, *f*), such reflections form a nearly horizontal track.

During the storm main and recovery phases, the G effect was recorded at the Irkutsk station, as at the Novosibirsk station: f_oF1>f_oF2. It was observed during the local daytime for three hours (22–01 UT) on May 10–11 and for ten hours (22–08 UT) on May 11–12.

On May 11 from 10:00 to 10:30 UT at sunset, the dusk enhancement of F2-layer electron density and peak height was detected in VS ionograms (Figure 5, *g*). As noted above, the convection field strength during this period decreased abruptly to an average level under quiet conditions, and then increased sharply (see Figure 3, *e*).

Figure 6 presents VS ionograms with the results of reconstruction of HFC *h'*(*f*) and plasma frequency profile $f_e(h)$ [Grozov et al., 2012; Ponomarchuk et al., 2023], which illustrate quantitative changes in the F2-layer critical frequency and peak height during the dusk effect.

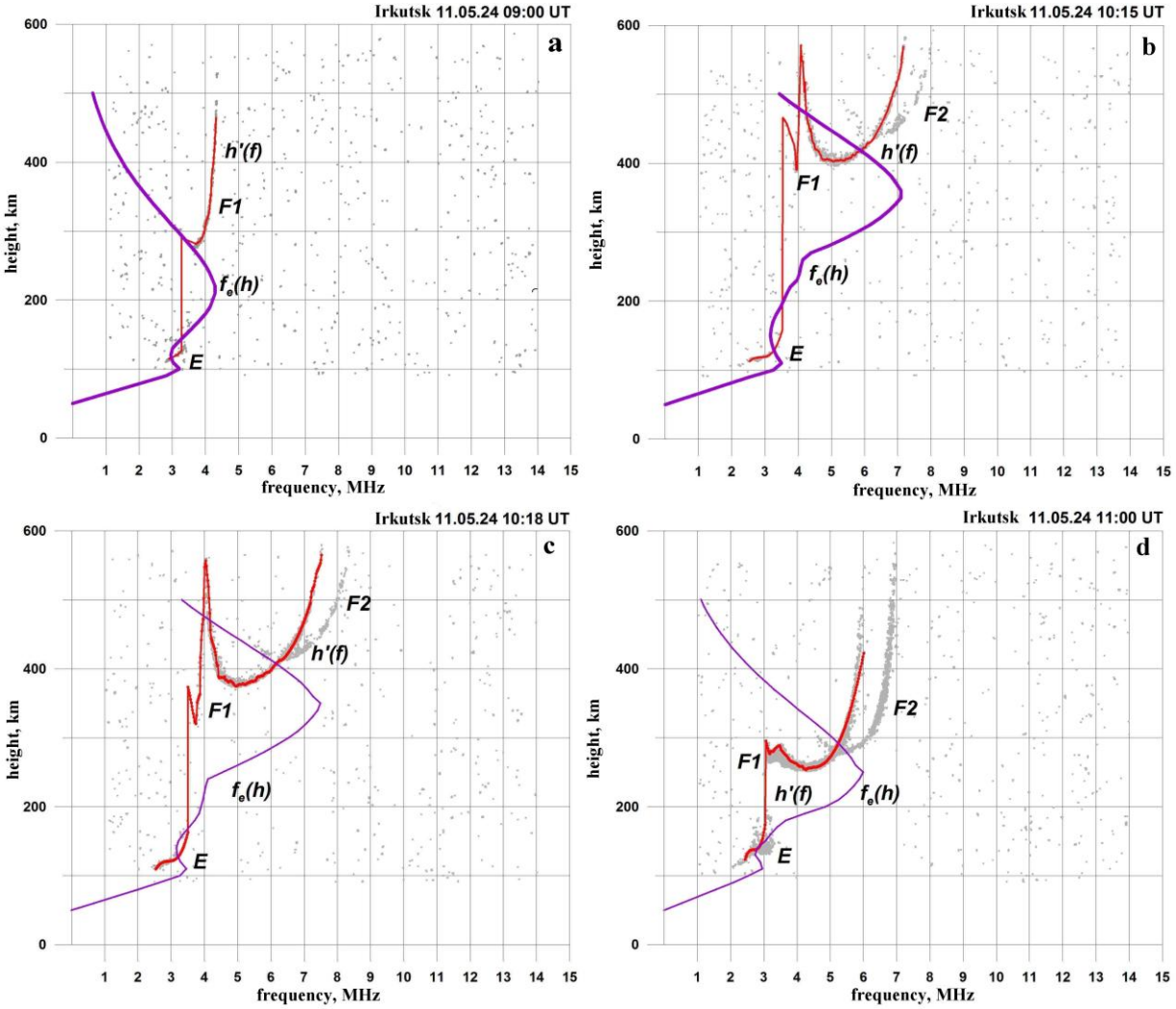

Figure 6. VS ionograms (gray dots), height-frequency characteristics *h'*(*f*) (red lines), and plasma frequency profiles $f_e(h)$ (dark red lines): the Irkutsk station, May 11, 2024

Signals reflected from the F1 and E layers were recorded on May 11, 2024 at 09:00 UT (Figure 6, *a*). The F1-layer critical frequency was 4.3 MHz; its peak height, 215 km. There are no reflections from the F-region between 09:39 and 09:44 UT. Then, a track of signals reflected from the F2 layer appears in the ionogram of vertical sounding with an ionosonde near the upper boundary (600 km). The track is characterized by a large virtual height of the beginning of the layer. The signals reflected from the F1 layer are absent or faint in the ionogram. Hence there is no G effect. From 10:03 UT, along with reflections from the F2 layer there are signals reflected from the F1 layer, and HFC of VS signals looks like that in the 10:15 UT ionogram in Figure 6, *b*. The F2-layer critical frequency increases: f_oF2=7.17 MHz. The F2-layer peak height also increases: h_mF2=350 km. At 10:18 UT, there are maximum values of f_oF2=7.52 MHz and h_mF2=354 km. Then, the F2-layer critical frequency and peak height decrease. At 11:00 UT, f_oF2=6.0 MHz, h_m F2=246 km (Figure 6, *d*).

3.1.3. Features of ionospheric disturbances according to VS data

1. During the storm main and recovery phases, a long-lasting negative ionospheric disturbance occurred which revealed itself in a significant reduction of F2-layer critical frequencies. Extreme deviation of f_oF2 from background values was ~75 %. At the same time, the F1-layer critical frequencies decreased only on May 11 and 12. Extreme deviation of f_oF1 from background values was ~25 %.

2. During the storm main and recovery phases, there were intervals without reflections from the F2 layer, associated with low electron content of this layer and increased radio wave absorption at low frequencies, close to the electron gyrofrequency, as well as with shielding of the F2 layer by the F1 or E_s layers.

3. During the storm main and recovery phases, auroral E_s layers and extended oblique E_s layers caused by electron precipitation at the inner plasma sheet boundary were recorded at the Novosibirsk station. The Irkutsk station registered auroral or delayed E_s layers.

4. During the storm main and recovery phases on May 11 and 12, the G effect was observed at both stations during the local daytime hours when the F1-layer critical frequency exceeded the F2-layer critical frequency. On May 12, the continuous observation interval

of the G effect at the Irkutsk station was 10 hrs; at the Novosibirsk station, 8 hrs.

5. At sunset on May 11, 2024, the dusk enhancement of F2-layer electron density and peak height was recorded in VS ionograms of both stations. During this time, the convection field strength decreased sharply to almost its average level under quiet conditions, and then increased abruptly, which might have brought about the dusk effect.

3.2. Ionospheric disturbances according to OS data

Figure 2 presents a diagram of oblique sounding radio paths in the Asian region of Russia. The preliminary results of OS data analysis are set forth in [Yasyukevich et al., 2025]. It has been found that negative ionospheric disturbances during the superstorm main and recovery phases caused a significant reduction of maximum observed frequencies relative to their level under quiet conditions and an increase in radio wave absorption, which together led to a weakening of signals and to long blackout intervals. Below are the results of a more detailed investigation into peculiarities of manifestation of the magnetosphere-ionosphere coupling during the May 10–13, 2024 magnetic storm in OS data.

3.2.1. Novosibirsk—Irkutsk path

First, we examine the OS path Novosibirsk—Irkutsk. Since this path is short, the main features of changes in ionospheric parameters at transmitting and receiving points will also manifest themselves in variations of maximum observed frequencies of propagation modes for signals reflected from the E, F1, F2, and E_s layers.

Figure 7 illustrates variations in experimental MOFs of 1F2, 1F1, 2F2, $1E_s$ propagation modes under disturbed and quiet conditions, and presents OS ionograms from the Novosibirsk—Irkutsk path. Ionospheric disturbances during the storm main phase revealed themselves in radio wave propagation conditions on May 10 from 17:50 UT when spread-F of regular propagation modes 1F2 and 2F2 was recorded in OS ionograms (Figure 7, *e*). At this time, the magnetospheric convection field increased sharply, which resulted in a shift of MIT and the diffuse electron precipitation zone to the region of OS signal propagation and reflection along the Novosibirsk—Irkutsk path (see Figures 3, *d* and 5, *d*). The shift of MIT gave rise to additional diffuse signals, reflected from the MIT polar wall, along with signals of regular propagation modes in OS ionograms. In the ionogram received on May 10 at 18:25 UT (Figure 7, *e*), such signals are designated as 1s and 2s.

Later, regular propagation modes 1F2 and 2F2 in the ionograms disappeared due to the lower concentration in the F2 layer and the corresponding increased absorption at low frequencies. Signals scattered by ionospheric irregularities in the diffuse precipitation zone near the MIT polar wall and signals reflected from the E_s layer were recorded (see the 19:46 UT ionogram in Figure 7, *e*).

During the storm early recovery phase, the reflecting ionospheric region was located in the MIT zone; therefore, there were weak diffuse signals of regular one-hop propagation modes and signals reflected from the type f flat E_s layer in the OS ionograms (see Figure 7, *e*).

The dusk effect in the ionosphere on May 11 at 10–11 UT (see Figures 3, *h* and 5, *g*), described in Subsections 3.1.1 and 3.1.2, was also recorded in OS ionograms from the Novosibirsk—Irkutsk path as increasing 1F2 MOF relative to the negative disturbance (Figure 7, *a*). In the ionogram on May 11 at 10:44 UT (Figure 7, *f*), there are signals reflected from the F1 and F2 layers.

The G effect observed at the Novosibirsk and Irkutsk stations (Figure 7, *a*, *b*) appeared in OS ionograms in the absence of signals reflected from the F2 layer, i.e. there was only a waveguide propagation channel formed by the Earth surface and F1 layer [Ponomarchuk et al., 2024].

A change in the mode structure of HF signals during the storm recovery phase is shown by OS ionograms in Figure 7, *g*. At 00:38 UT (during local morning hours) on May 12, 2024 when the G effect was observed at the Novosibirsk and Irkutsk stations, one-hop modes 1F1 and $1E_s$ were registered. During local midday hours, signals reflected once from the F2 layer were additionally recorded in OS ionograms; and in the evening, 2F2 and 1E propagation modes.

3.2.2. Magadan—Irkutsk

Figure 8 displays variations in experimental MOFs of 1F2, 1F1, 2F2, $2E_s$ propagation modes under disturbed and quiet conditions, variations in invariant latitudes of the MIT bottom and DPB at 120° E, and OS ionograms from the Magadan—Irkutsk path. Horizontal dotted lines in Figure 8, *e* indicate the invariant latitudes of midpoints of the Magadan—Irkutsk (Φ=53.39°) and Magadan—Novosibirsk (Φ=57.77°) radio paths at an altitude of 250 km.

As noted above, a negative ionospheric disturbance can cause critical frequencies of reflecting ionospheric layers to decrease during the storm main and recovery phases, there is, therefore, a significant reduction of maximum observed frequencies as compared to quiet conditions. Since a decrease in the frequency of recorded signals leads to an increase in radio wave absorption, weak signals and long blackout intervals are recorded during the storm main and recovery phases (Figure 8, *a*, *b*). As along the Novosibirsk—Irkutsk path, weak diffuse regular propagation modes 1F2 and 2F2 were recorded in OS ionograms from the Magadan—Irkutsk path on May 10 from 17:50 UT (Figure 8, *f*). The magnetospheric convection field increases sharply (see Figure 3, *e*), which results in a shift of MIT and diffuse electron precipitation zone to the region of propagation and reflection of OS signals along the Magadan—Irkutsk path (Figure 8, *e*). Heights of diffuse signal reflection from the F2 layer increase, as can be seen in the 18:20 UT ionogram in Figure 8, *f*. During the local dusk-dawn hours on May 11 and 12, the middle (reflecting signals) part of the radio path was in the MIT zone; therefore, long blackout intervals alternated with periods of recording signals reflected from the F1 and E_s layers, as in the ionogram on May 11, 2024 at 00:00 UT.

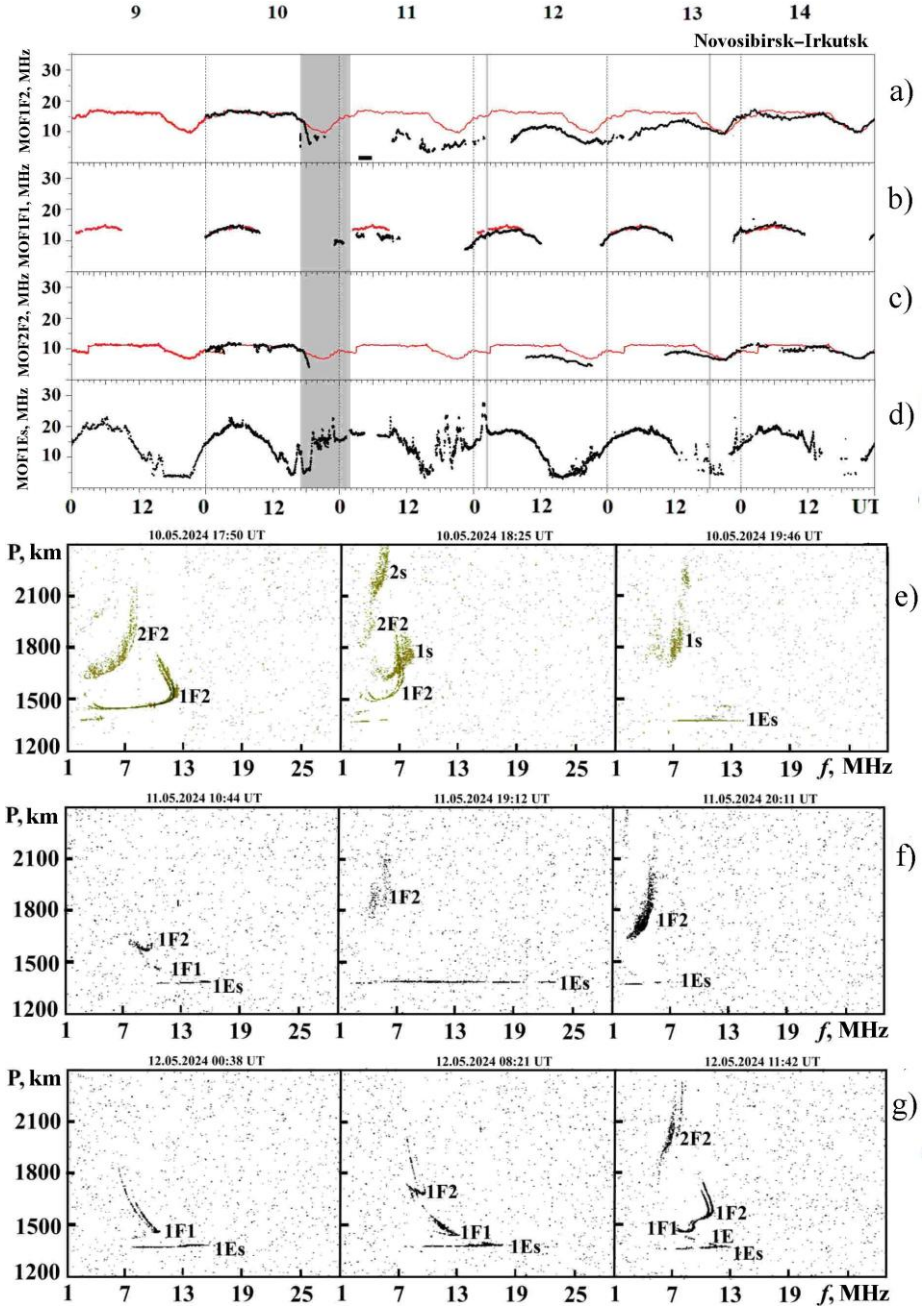

Figure 7. Variations in experimental MOFs of 1F2, 1F1, 2F2, $1E_s$ propagation modes under disturbed (black dots) and quiet (red line) conditions on May 9–14, 2024 (*a*–*d*) and OS ionograms from the Novosibirsk—Irkutsk path for May 10–12, 2024 (*e*–*g*)

The G effect in OS data from the Magadan—Irkutsk path appeared on May 11 and 12 at the same time when it was recorded in VS data from the Irkutsk station and in OS data from the Novosibirsk—Irkutsk path (see Figures 5 *a*, *b* and 8, *a*–*c*), which is natural because there was no waveguide channel for signal propagation by reflection from the F2 layer at the receiving point during these hours: the F1 layer shielded the F2 layer along the propagation path [Ponomarchuk et al., 2024].

Figure 8, *g* presents OS ionograms illustrating a change in the mode structure of HF signals during G-effect transitional hours. At 09:35 UT (16:35 LT), along with the 1F1 propagation mode there is the 1F2 mode in the ionogram. At 15:25 UT (22:25 LT), only the 1F2 and 2F2 propagation modes are observed in the ionogram. At 22:00 UT (05:00 LT), the 1F1 and 1F2 propagation modes are registered in the ionogram.

3.2.3. Magadan—Novosibirsk

During the superstorm main and recovery phases, the initial part of the radio path together with the transmitting station was located in the auroral zone; and the middle part of the path (invariant latitude of the midpoint Φ=57.77°), in the MIT region. A decrease in the critical frequencies of the reflecting ionospheric layers caused a significant decrease in MOF as compared to quiet conditions and an increase in radio wave absorption, which together led to an attenuation of signals of 1F2, 1F1, 2F2 propagation modes and to long blackout intervals (Figure 9, *a*–*c*). Along this path, the G effect was observed on May 13 only at 00:00–04:30 UT.

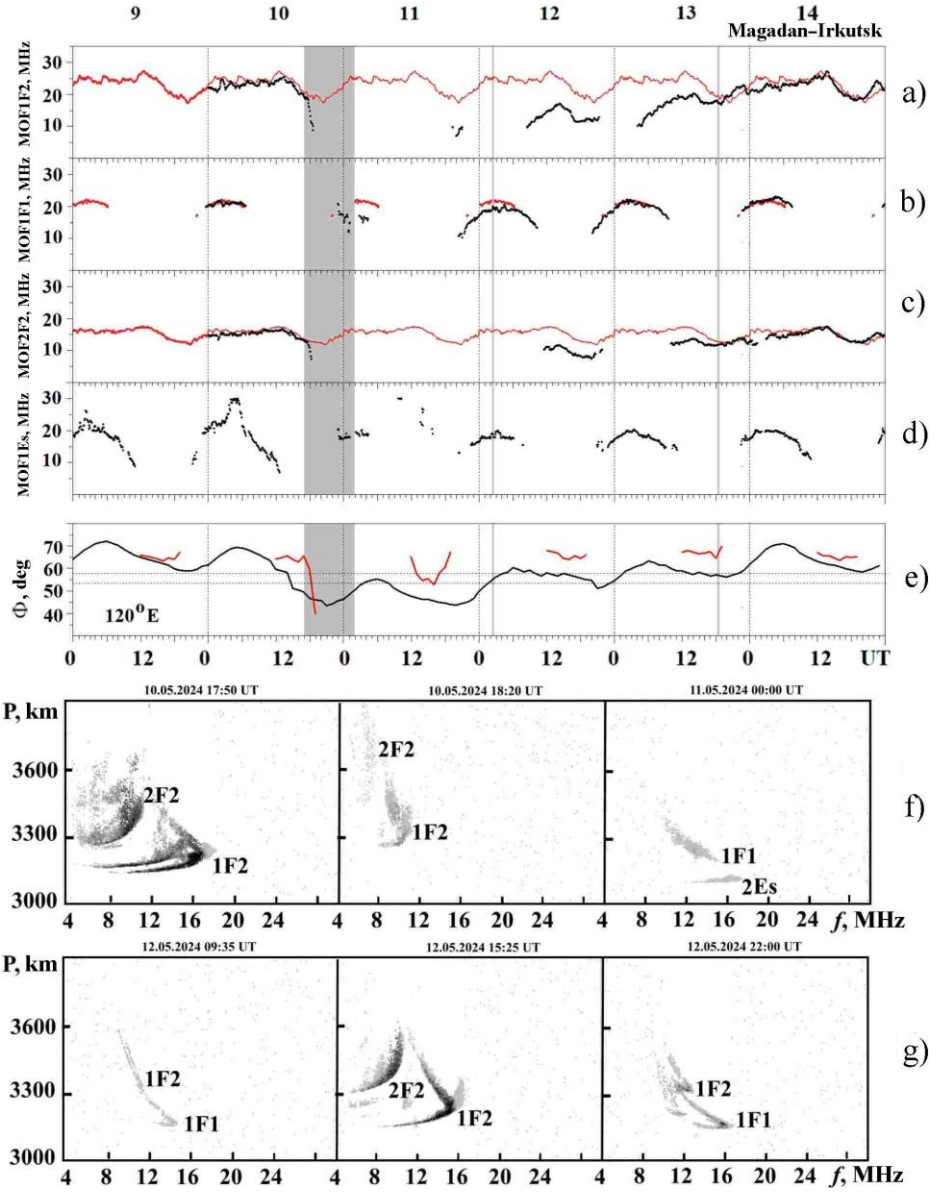

Figure 8. Variations in experimental MOFs of 1F2, 1F1, 2F2, $2E_s$ propagation modes in disturbed (black dots) and quiet (red line) conditions (*a*–*d*); variations in invariant latitudes of the MIT bottom (black line) and DPB (red line) at 120° E (*e*) on May 9–14, 2024, and OS ionograms from the Magadan—Irkutsk path for May 10–12 (*f*, *g*)

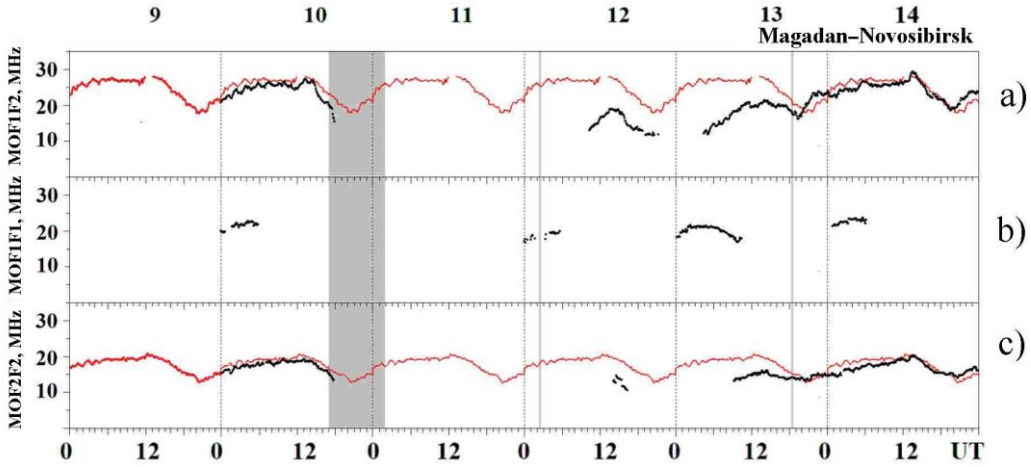

Figure 9. Variations in experimental MOFs of propagation modes 1F2 (*a*), 1F1 (*b*), 2F2 (*c*) on May 9–14, 2024 under disturbed (black dots) and quiet (red line) conditions

3.2.4. Features of ionospheric disturbances according to OS data

1. During the storm main and recovery phases, the long-lasting negative ionospheric disturbance caused a decrease in maximum observed frequencies relative to those under quiet conditions and an increase in radio wave absorption, which together led to a weakening of reflected signals and to long blackout intervals.

2. During the storm main and recovery phases, the strengthening of the magnetospheric convection field caused MIT and DPB to shift to latitudes of reflecting regions of the radio paths, and radio wave propagation conditions became similar to subauroral. Changes in characteristics of radio wave propagation along the radio paths are associated with off-angle reflections of signals from the MIT polar wall and scattering of radio waves by ionospheric irregularities in the diffuse electron precipitation zone.

3. The periods of manifestation of the G effect in ionospheric parameters (f_oF1>f_oF2) closely matched the recording intervals of signals reflected only from the F1 layer in OS ionograms.

4. Along the Novosibirsk—Irkutsk path in OS data on May 11 near 10–11 UT, the manifestation of the dusk effect was recorded as increasing 1F2 MOF against low values of this parameter.

CONCLUSION

We have examined the effects of the May 10–13, 2024 magnetic storm, which revealed themselves as ionospheric disturbances that changed HF radio wave propagation conditions. Magnetosphere-ionosphere coupling features in data from vertical and oblique sounding with a continuous chirp signal have been identified. Experimental data was analyzed using empirical models of invariant latitudes of the MIT bottom and the equatorial boundary of the zone of diffuse precipitation of ≥100 eV electrons and the model of magnetospheric convection field strength. We have also employed data on spatial TEC distribution and DMSP satellite data. The following features of ionospheric disturbances caused by the great magnetic storm have been identified.

1. During the storm main and recovery phases, a long-lasting negative ionospheric disturbance, which manifested itself as a significant decrease in F2-layer critical frequencies, caused a reduction of maximum observed frequencies along radio paths relative to their values under quiet conditions and an increase in radio wave absorption. An increase in the electric field of magnetospheric convection during this period led to a shift of the main ionospheric trough and the diffuse electron precipitation zone to the latitudes of VS stations and transceivers, as well as middle (reflecting signals) parts of radio paths. During dusk and night hours, additional diffuse signals reflected from the MIT polar wall were recorded in VS and OS ionograms. There were long blackout intervals.

2. During the storm main and early recovery phases, there were intervals without reflections from the F-region of the ionosphere due to shielding by the E_s layer and increased absorption at low frequencies close to the electron gyrofrequency. Auroral E_s layers and extended oblique E_s layers produced by electron precipitation at the inner plasma sheet boundary were observed at the VS station in Novosibirsk. The Irkutsk station recorded E_s layers of auroral and delayed types.

3. During the storm recovery phase, the G effect was observed at the VS stations during local daytime hours when the F1-layer critical frequency exceeded the F2-layer critical frequency. In OS ionograms, the G effect revealed itself in the absence of signals reflected from the F2 layer.

4. On May 11, the dusk enhancement of F2-layer electron density and peak height was recorded in VS ionograms. Along the OS path Novosibirsk—Irkutsk, the dusk effect showed itself as an increase in 1F2 MOF against the background of its lower values.

The work was financially supported by the Ministry of Science and Higher Education of the Russian Federation (Projects FWSE-2021-0002, FWZZ-2022-0019). The experimental data was obtained using the equipment of Shared Equipment Center «Angara» [http://ckp-rf.ru/ckp/3056/].

REFERENCES

Benkova N.P., Kozlov E.F., Kochenova N.A., Samorokin N.I., Fligel M.D. Structure and Dynamics of the Subauroral Ionosphere. Moscow, Nauka Publ., 1993, 144 p. (In Russian).

Besprozvannaya A.S., Ben'kova N.P. Large-scale structural features of the F2 layer at high latitudes. *Proc. of International Symposium "Physical Processes in the Trough Region during Disturbances". Garzau, GDR (31.03 – 04.04.1987).* Berlin, 1988, pp. 25–39. (In Russian).

Bilitza D., Pezzopane M., Truhlik V., Altadill D., Reinisch B. W., Pignalberi A. The International Reference Ionosphere model: A review and description of an ionospheric benchmark. *Rev. Geophys*. 2022, vol. 60, no. 4, p. e2022RG000792. DOI: 10.1029/2022RG000792.

Blanch E., Altadill D., Boska J., Burešová D., Hernández-Pajares M. November 2003 event: Effects on the Earth's ionosphere observed from ground-based ionosonde and GPS data. *Ann. Geophys*. 2005, vol. 23, no. 9. pp. 3027–3034. DOI: 10.5194/angeo-23-3027-2005.

Buonsanto M.J. A case study of the ionospheric storm dusk effect. *J. Geophys. Res.: Space Phys*. 1995, vol. 100, no. A12, pp. 23857–23869. DOI: 10.1029/95JA02697.

Burke W.J., Huang C.Y., Marcos F.A., Wise J.O. Interplanetary control of thermospheric densities during large magnetic storms. *J. Atmos. Solar-Terr. Phys*. 2007, vol. 69, iss. 3, pp. 279–287. DOI: 10.1016/j.jastp.2006.05.027.

Collado-Villaverde A., Muñoz P., Cid C. Classifying and bounding geomagnetic storms based on the *SYM-H* and *ASY-H* indices. *Natural Hazards*. 2024, vol. 120, no. 2. pp. 1141–1162. DOI: 10.1007/s11069-023-06241-1.

Daglis I.A. The storm-time ring current. *Space Sci. Rev*. 2001, vol. 98, no. 3, pp. 343–363. DOI: 10.1023/A:1013873329054.

Deminov M.G., Romanova E.B., Tashchilin A.V. Origination of G conditions in the ionospheric F region depending on solar and geomagnetic activity. *Geomagnetism and Aeronomy*. 2011, vol. 51, no. 5, pp. 669–675.

Deminov M.G., Shubin V.N. Empirical model of the location of the main ionospheric trough. *Geomagnetism and Aeronomy*. 2018, vol. 58, no. 3, pp. 348–355. DOI: 10.1134/S0016793218030064.

Echer E., Gonzalez W.D., Tsurutani B.T. Interplanetary conditions leading to superintense geomagnetic storms (*Dst*≤–250 nT) during solar cycle 23. *Geophys. Res. Lett*. 2008, vol. 35, no. 6, L06S03. DOI: 10.1029/2007GL031755.

Fang X., Randall C.E., Lummerzheim D., Solomon S.C.,

Mills M.J., Marsh D.R., et al. Electron impact ionization: A new parameterization for 100 eV to 1 MeV electrons. *J. Geophys. Res.: Space Phys*. 2008, vol. 113, A09311. DOI: 10.1029/2008JA013384.

Galperin Yu.I. , Crasnier J., Sauvaud J.-A., Lisakov Iu.V., Nikolaenko L.M., Sinitsyn V.M., Khalipov V.L. The diffuse auroral zone. I – Model of the equatorial boundary of diffuse auroral electron precipitation zone in the evening and near midnight sectors. *Kosmicheskie issledovaniya* [Cosmic Res]. 1977, vol. 15, no. 3, pp. 421–434. (In Russian).

Gonzalez W.D., Joselyn J.A., Kamide Y., Kroehl H.W., Rostoker G., Tsurutani B.T., Vasyliunas V.M. What is a geomagnetic storm? *J. Geophys. Res.: Space Phys*. 1994, vol. 99, no. A4, pp. 5771–5792. DOI: 10.1029/93JA02867.

Grozov V.P., Ilyin N.V., Kotovich G.V., Ponomarchuk S.N. Software system for automatic interpretation of ionosphere sounding data. *Pattern Recognition and Image Analysis*. 2012, vol. 22, no. 3, pp. 458–463. DOI: 10.1134/S1054661812030042.

Khalipov V.L., Galperin Yu.I., Lisakov Yu.V., et al. Diffuse auroral zone. II. Formation and dynamics of the polar edge of the subauroral ionospheric trough in the evening sector. *Kosmicheskie issledovaniya* [Cosmic Res]. 1977, vol. 15, no. 5, pp. 708–723. (In Russian).

Iyemori T., Rao D.R.K. Decay of the *Dst* field of geomagnetic disturbance after substorm onset and its implication to storm-substorm relation. *Ann. Geophys.* 1996, vol. 14, no. 11, pp. 608–618. DOI: 10.1007/s00585-996-0608-3.

Kamide Y., Winningham J.D. A statistical study of the "instantaneous" nightside auroral oval: The equatorward boundary of electron precipitation as observed by the Isis 1 and 2 satellites. *J. Geophys. Res*. 1977, vol. 82, iss. 35, pp. 5573–5588. DOI: 10.1029/JA082i035p05573.

Kurkin V.I., Ponomarchuk S.N., Smirnov V.F. On the influence of the main ionospheric trough on the characteristics of HF signals on oblique sounding paths. *Solnechno-zemnaya fizika* [Sol.-Terr. Phys.]. 2004, no. 5, pp. 124–127. (In Russian).

Kurkin V.I., Zolotukhina N.A., Ponomarchuk S.N., Oinats A.V., Ratovskii K.G. Specific features of ionospheric disturbances accompanying the magnetic storm of January 14–20, 2022. *Geomagnetism and Aeronomy*. 2024a, vol. 64, no. 6, pp. 869–880. DOI: 10.1134/S0016793224600784.

Kurkin V.I., Medvedeva I.V., Podlesnyi A.V. Effect of sudden stratosphere warming on characteristics of medium-scale traveling ionospheric disturbances in the Asian region of Russia. *Adv. Space Res*. 2024b, vol. 73, no. 7, pp. 3613–3623. DOI: 10.1016/j.asr.2023.09.020.

Laryunin O.A., Kurkin V.I., Rybkina A.A., Podlesnyi A.V. Determination of the velocity of ionospheric disturbances from the dynamics of additional U-shaped traces on ionograms. *Geomagnetism and Aeronomy*. 2024, vol. 64, no. 2, pp. 235–241. DOI: 10.1134/S0016793223601084.

Loewe C.A., Prolss G.W. Classification and mean behavior of magnetic storm. *J. Geophys. Res*. 1997, vol. 102, no. A7, pp. 14209–14213. DOI: 10.1029/96JA04020.

Mikhailov S.Ya. Ambiguity of the reconstruction of plasma frequency profiles from a given height-frequency characteristic and their discernibility for oblique propagation of HF radio waves in an isotropic ionosphere. *Radiophysics and Quantum Electronics*. 2000, vol. 43, no. 10, pp. 766–782.

Mishin V.V., Lunyushkin S.B., Mikhalev A.V., Klibanova Yu.Yu., Tsegmed B., Karavaev Yu.A., et al. Extreme geomagnetic and optical disturbances over Irkutsk during the 2003 November 20 superstorm. *J. Atmos. Solar-Terr. Phys*. 2018, vol. 181, pp. 68–78. DOI: 10.1016/j.jastp.2018.10.013.

Möller H.G. Backscatter results from Lindau-II. The movement of curtains of intense irregularities in the polar F-layer. *J. Atmos. Terr. Phys*. 1974, vol. 36, no. 9, pp. 1487–1501. DOI: 10.1016/0021-9169(74)90227-X.

Nishida A. *Geomagnetic diagnosis of the magnetosphere*. Springer Nature, 1978, 256 p.

Panasyuk M.I., Kuznetsov S.N., Lazutin L.L., Alexeev I.I., Antonova A.E., Belenkaya E.S., et al. Magnetic storms in October 2003. *Cosmic Res*. 2004, vol. 42, no. 5, pp. 489–534.

Pavlov A.V. Vibrationally excited N_2 and O_2 in the upper atmosphere: A review. *Geomagnetism and Aeronomy*. 2011, vol. 51, no. 2, pp. 143–169. DOI: 10.1134/S0016793211020149.

Pilkington G.R., Münch J.W., Braun H.J., Möller H.G. Comparison of ground HF backscatter and simultaneous particle and plasma pause measurements from a polar orbiting satellite. *J. Atmos. Terr. Phys*. 1975, vol. 37, no. 2, pp. 337–347. DOI: 10.1016/0021-9169(75)90115-4.

Pirog O.M., Polekh N.M., Romanova E.B., Tashchilin A.V., Zherebtsov G.A. The main ionospheric trough in the East Asian region: Observation and modeling. *J. Atmos. Solar-Terr. Phys*. 2009, vol. 71, no. 1, pp. 49–60. DOI: 10.1016/j.jastp.2008.10.010.

Podlesny A.V., Brynko I.G., Kurkin V.I., Berezovsky V.A., Kiselyov A.M., Petukhov E.V. Multifunctional chirp ionosonde for monitoring the ionosphere. *Geliogeofizicheskie issledovaniya* [Heliogeophysical research]. 2013, no. 4, pp. 24–31. (In Russian).

Polekh N.M., Ratovsky K.G., Deminov M.G., Kolpakova O.E., Kushnarenko G.P. Morphology of the G condition occurrence over Irkutsk. *Adv. Space Res*. 2013, vol. 52, no. 4, pp. 575–580. DOI: 10.1016/j.asr.2013.04.013.

Polekh N.M., Romanova T.B., Ratovsky K.G., Shi J.K., Wang X., Wang G.J. Studying the G condition occurrence in different latitudes under solar minimum: Observation and modeling. *J. Atmos. Solar-Terr. Phys*. 2015, vol. 130, no. 8, pp. 132–141. DOI: 10.1016/j.jastp.2015.06.001.

Ponomarchuk S.N., Grozov V.P. Automatic interpretation of oblique sounding ionograms based on hybrid algorithms. *Sol.-Terr. Phys*. 2024, vol. 10, iss. 2, pp. 102–110. DOI: 10.12737/stp-102202410.

Ponomarchuk S.N., Zolotukhina N.A. Disturbances of ionospheric radio channel during magnetic storms in November–December 2023. *Sol.-Terr. Phys*. 2024, vol. 10, no. 4, pp. 84–98. DOI: 10.12737/stp-104202410.

Ponomarchuk S.N., Grozov V.P., Kotovich G.V. Technique of ionospheric parameters automatic determination from data of vertical sounding with a continuous chirp signal. *Proc. SPIE 12780: 29th International Symposium on Atmospheric and Ocean Optics: Atmospheric Physics*. 2023, 127806Q. DOI: 10.1117/12.2688438.

Ponomarchuk S.N., Kurkin V.I., Ilyin N.V., Penzin M.S. HF radio path modeling by waveguide approach. *Sol.-Terr.*

Phys. 2024, vol. 10, no. 2, pp. 93–101. DOI: 10.12737/stp-102202409.

Prölss G.W., Brace L.H., Mayr H.G., Carignan G.R., Killeen T.L., Klobuchar J.A. Ionospheric storm effects at subauroral latitudes: A case study. *J. Geophys. Res.: Space Phys*. 1991, vol. 96, no. A2, pp. 1275–1288. DOI: 10.1029/90JA02326.

Sergeev V.A., Tsyganenko N.A. *Magnitosfera Zemli* [Earth's magnetosphere]. Moscow, Nauka Publ., 1980, 174 p. (In Russian).

Spogli L., Alberti T., Bagiacchi P., Cafarella L., Cesaroni C., Cianchini G., et al. The effects of the May 2024 Mother's Day superstorm over the Mediterranean sector: from data to public communication. *Ann. Geophys*. 2024, vol. 67, no. 2, PA218. DOI: 10.4401/ag-9117.

Tashchilin A.V., Romanova E.B. Role of magnetospheric convection and precipitation in the formation of the "dusk effect" during the main phase of a magnetic storm. *Geomagnetism and Aeronomy*. 2011, vol. 51, no. 4, pp. 468–474. DOI: 10.1134/S0016793211040074.

Uryadov V.P., Kurkin V.I., Vertogradov G.G., Vertogradov V.G., Ponyatov A.A., Ponomarchuk S.N. Features of propagation of HF signals on mid-latitude paths under conditions of geomagnetic disturbances. *Radiophysics and Quantum Electronics*. 2004, vol. 47, no. 12, pp. 933–946.

Uryadov V.P., Ponyatov A.A., Vertogradov G.G., Vertogradov V.G., Kurkin V.I., Ponomarchuk S.N. Dynamics of the auroral oval during geomagnetic disturbances observed by oblique sounding of the ionosphere in the Eurasian longitudinal sector. *Int. J. Geomagn. Aeron*. 2005, vol. 6, GI1002. DOI: 10.1029/2004GI000078.

URSI Handbook of Ionogram Interpretation and Reduction. Second edition. November 1972. 335 p.

Yasyukevich Yu.A., Vasiliev R.V., Rubtsov A.V., Alsatkin S.S., Artamonov M.F., Beletsky A.B., et al. Extreme magnetic storm of May 10–19, 2024: Coupling between neutral and charged components of the upper atmosphere and the effect on radio systems. *Doklady Earth Sciences*. 2025, vol. 520, no. 33.
DOI: 10.1134/S1028334X24604978.

Zhang Y., Paxton L.J. An empirical K_p-dependent global auroral model based on TIMED/GUVI FUV data. *J. Atmos. Solar-Terr. Phys*. 2008, vol. 70, no. 8-9, pp. 1231–1242. DOI: 10.1016/j.jastp.2008.03.008.

Zherebtsov G.A., Mizun Yu.G., Mingalev V.S. Physical Processes in the Polar Ionosphere. Moscow, Nauka Publ., 1988, 232 p. (In Russian).

Zherebtsov G.A., Pirog O.M., Polekh N.M. The ionospheric situation in the Eastern Asian longitudinal sector during the geoactive period October–November 2003. *Geomagnetism and Aeronomy*. 2005, vol. 45, no. 1, pp. 101–108.

URL: https://cdaweb.gsfc.nasa.gov (accessed May 14, 2025).

URL: https://cdaw.gsfc.nasa.gov/CME_list/ (accessed May 14, 2025).

URL: https://kp.gfz-potsdam.de/en/data (accessed May 14, 2025).

URL: https://ssusi.jhuapl.edu/gal_edr-aur_cs (accessed May 14, 2025).

URL: https://wdc.kugi.kyoto-u.ac.jp/dst_provisional/index.html (accessed May 14, 2025).

URL: https://www.swpc.noaa.gov/noaa-scales-explanation (accessed May 14, 2025).

URL: http://ckp-rf.ru/ckp/3056/ (accessed May 14, 2025).

Original Russian version: Ponomarchuk S.N., Zolotukhina N.A., Kurkin V.I., Belinskaya A.Yu., Grozov V.P., Oinats A.V., Poddelsky A.I., Podlesnyi A.V., Cedrik M.V., published in Solnechno-zemnaya fizika. 2025, vol. 11, no. 4, pp. 17–32. DOI: 10.12737/szf-114202504.

How to cite this article

Ponomarchuk S.N., Zolotukhina N.A., Kurkin V.I., Belinskaya A.Yu., Grozov V.P., Oinats A.V., Poddelsky A.I., Podlesnyi A.V., Cedrik M.V. Effects of the May 10–13, 2024 magnetic storm in the Asian region of Russia from ionospheric sounding with a continuous chirp signal. *Sol.-Terr. Phys*. 2025, vol. 11, iss. 4, pp. 14–28. DOI: 10.12737/stp-114202504.